Aridity synthesis for 10 selected key regions of the global climate system during the last 60 000 years

Florian Fuhrmann[1], Benedikt Diensberg[1], Xun Gong[2], Gerrit Lohmann[2], Frank Sirocko[1]

[1]Department for Geoscience, Johannes-Gutenberg-Universität, Mainz, 55099, Germany

[2]Alfred Wegener Institute for Polar and Marine Research, Bremerhaven, Germany

Correspondence to: Florian Fuhrmann, (flfuhrma@uni-mainz.de)

Abstract. A compilation of published literature on the dust content in terrestrial and marine sediment cores are synchronised on the basis of pollen data and speleothem growth phases within GICC05 age constrain. Aridity patterns for ten key areas of the global climate system are reconstructed over the past 60 000 years. These records have different time resolutions and different dating methods, thus various types of stratigraphy. Nevertheless, all the regions analysed in this study show humid conditions during the early Marine Isotope Stage 3 (MIS3) and early Holocene, but not always with the same timing. Such discrepancies have been interpreted as regional effects, although stratigraphic uncertainties may affect some of the proposed interpretations. In comparison, most of the MIS2 interval becomes arid in all of the northern hemisphere records, but the peak arid conditions of the Last Glacial Maximum (LGM) and Heinrich event 1 differ in duration and intensity among regions. In addition, we also compare the aridity synthesis with modelling results using a Global Climate Model (GCM). Indeed, geological archives and GCMs show agreement of aridity pattern for the Holocene, LGM and for the late MIS3.

1 Introduction

Paleoclimate research today has two main foci: i) well dated, high resolution archives of past climate (e.g., marine and terrestrial sediments, speleothems, tree rings and ice cores), ii) modelling of global and regional characteristics with Global Climate Models (GCM), which include main processes in atmosphere, ocean, land and cryosphere as well as their coupling. Geological archives have the potential to provide information on the past states of climate variables at the global and regional level, and their evolution in time. The strength of modelling approach, on the other hand, is to understand the processes of climate change and global teleconnections. A reliable model of past climate change should faithfully reproduce the observed climate patterns as reconstructed from geo-archives. We will test this prerequisite for a set of records that approximating past global aridity.

This paper emerges from the PalMod project which develops a long GCM time series of past global temperatures (www.palmod.de),. One prerequisite of the project was to work only with publically available datasets from the most cited papers. Thus, we had to use only available datasets from publically accessible databases (PANGAEA, NOAA-NCDC,

Neotoma (global pollen database), ice core database from Copenhagen university, SISAL (speleothem database) and EPD (European pollen database)) by citation count. The most complete, highly cited and well dated (back to 60 000 yr b2k) records with high sample resolution were used for the aridity index calculation. We could not incorporate those records into the aridity index calculation, which do not fulfil this prerequisites (see the compilation of prerequisites above). All data were plotted on the age scale b2k.

We use continuous time series that cover the Holocene, 0 - 11 700 years before 2000 CE (yr b2k), Marine Isotope Stage 2 (MIS2) (24 000 - 12 500 yr b2k) and also the flickering climate of MIS3 (60 000 – 24 000 yr b2k).The boundaries of the MIS have been developed by Imbrie et al. (1984) and Martinson et al. (1987) with refinements by Thompson and Goldstein (2006).

In this paper, we concentrate on published paleoclimate reconstructions for aridity, which is one of the most important indicators of climate change. We have screened published paleoclimate literature of the last 30 years to detect and select 10 key areas. These key areas were defined by the proxy availability, i.e. pollen, dust and speleothem growth must provide three independent sources of information related to past precipitation. These areas were selected because they were the smallest possible regions meeting the following criteria: i) publically available datasets from data repositories, ii) highly cited, iii) well dated, iv) sufficient sample resolution (as far back as possible to 60 000 yr b2k). Many important records of paleoclimatic research are thus not included in these 10 key regions, because only one or two of the aridity proxies are available or they are far away from complementary aridity records. Several high resolution records which extend into MIS3 (see. Fig. S11, dotted lines) are accessible from the literature but were not incorporated into this synthesis, because these cores were either too far away from the chosen ten key regions to fit into a suitable synthesis or cover only a small part of the last 60 000 years. Many other cores are excellent archives and will be discussed in this paper, but cannot be incorporated into the numerical calculation of the aridity index if data are not accessible from official data repositories. Sediment cores from e.g. Lake Tulane (Grimm et al., 2006), Bear Lake (Jiménez-Moreno et al., 2007), Lake Suigetsu (Bronk Ramsey et al., 2012), Petén-Itzá (Correa-Metrio et al., 2012) and Potrok Aike (Kliem et al., 2013) were not included in the aridity index as there were no other long time series with publically available datasets beside pollen within the region of the archive. The excellent loess archive of Nussloch (Antoine et al., 2001; Moine et al., 2017) could not be used for the synthesis because no accessible data were available in official data repositories. Even the excellent record of Dunaszekcso loess (Újvári et al., 2015) or pollen records from Tenaghi Phillipon (Pross et al., 2015) are not incorporated, because no data are available that covered at least a longer period of the last 60 000 years.

Dust is deflated only in regions with less than 200 mm/a precipitation, and thus indicate an arid climate (either subtropical or polar) (Pye, 1987). Speleothem growth needs dripping water in a cave, and thus rain or snow melt (Spötl and Mangini, 2002). Arboreal pollen implies more precipitation than in a landscape with abundant grass pollen. Accordingly, we do not evaluate the full width of information from these paleoclimate proxies, but just reduce the evidence to its basic structure, which is aridity. The most faithful aridity indicator is dust, which indicates deserts, whereas grass indicates steppic landscapes. Throughout this synthesis, we use ‘climate improvement’ for warmer and wetter climate conditions, whereas ‘climate deterioration’ (or similar terms) accord for colder and drier climate.

Figure 1 present the 10 key regions. The detailed evidence for each of the selected 10 key regions and their well dated and high-resolution proxy records are presented in Fig. 2 and Supplement S1-S9. The discussion compares the synoptic aridity reconstruction for the time of LGM (26 500 – 19 000 yr b2k), and late MIS3 (32 000 yr b2k, Fig. 4) with GCM simulations (Fig. 7, Tab. 3). Mix et al. (2001) define the LGM from comparably stable conditions during the time interval of 23 000 to 19 000 yr b2k. Clark et al. (2009) define the LGM by the maximum extend of the ice sheets and sea level low stand to 26 500 to 19 000 yr b2k for most parts of northern and southern hemisphere. We follow the wider definition of Clark et al. (2009), which encompasses the regional differences in the results of this work.

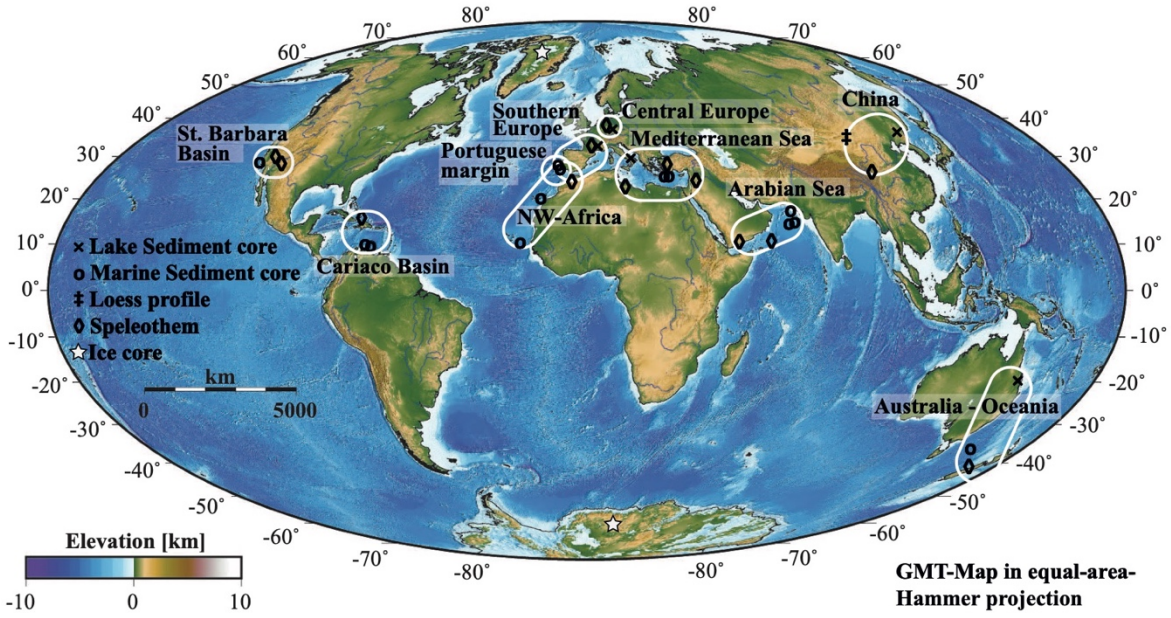

Figure 1: Global map with the 10 selected key regions and archive type, Generic Mapping Tool (GMT) (Wessel and Smith, 1991). Regions are indicated with white boundaries. Crosses sign lake sediment cores; open circles marine sediment cores; double sharp marks loess profile; Diamonds mark speleothems and white stars ice cores. The map is colour coded for the elevation.

We start the synthesis with Central Europe: Dust and pollen records from Eifel (Seelos et al., 2009; Sirocko et al., 2016), which we compare with speleothem data from nearby Bunker Cave (Fohlmeister et al., 2012, 2013; Weber et al., 2018) as well as the Spannagel Cave in Austria (Holzkämper et al., 2004, 2005; Spötl and Mangini, 2002), which shows a similar speleothem growth pattern. The maar sediment cores of the Eifel Laminated Sediment Archive (ELSA)-project (Sirocko et al., 2016) show all Greenland Stadials (GS) and Greenland Interstadials (GI) in the time series of eolian dust content (Dietrich and Sirocko, 2011; Seelos et al., 2009). Central Europe shows accordingly the same climatic structures, which are well known in North Atlantic marine sediments (e.g. Hodell et al., 2013; McManus et al., 1994; Naafs et al., 2013) and Greenland ice cores (North Greenland Ice Core Project Members et al., 2004; Rasmussen et al., 2014; Svensson et al., 2008). This Central European climate time series is then compared with the respective time series from all other 9 key regions, which data evidence is documented in the supplement.

2 Methods

The synthesis is based on pollen profiles from sediment cores, growth phases of speleothems and dust proxies like grain size of eolian fraction within sediment cores. Also, isotope data like $\delta^{18}O$, Sea Surface Temperature (SST) reconstructions or Ice Raft Debris (IRD) data are added to complete the interpretations within Figure 4 (for more details, see the supplement section). We used the original stratigraphy of all records on the age scale of yr b2k but we are aware of a general error of up to ± 2 000 years for all MIS 3 dates.

Especially the growth phases of speleothems are a significant indicator for presence of mobile water. If a speleothem could grow, at least some precipitation occurred over the cave. If a speleothem does not grow (hiatus), either no precipitation or a change of the drip water system above the cave could be causes. Most speleothem datasets also provide $\delta^{18}O$ or other isotope measurements (Genty et al., 2003; Hoffmann et al., 2016; Wainer et al., 2009) which often have local characteristics, thus our index only uses growth phases as the most common and robust aridity indicator.

Pollen are separated in two classes for this work. Trees and shrubs (in following only named tree pollen) were combined as they require similar climate conditions for their growth. Herbs and grasses (in following only named grass pollen) were also combined. Trees need a significantly larger amount of precipitation than grasses to grow. So, a simple statement about the relative precipitation of the catchment area of the core can be done by looking at the tree / grass pollen ratios. In general, a higher amount of tree pollen indicates warmer and wetter climate than high amounts of grass pollen. The time resolution of the pollen profiles is often low, but we have chosen the accessible highest resolution data of each selected region for the comparison.

The global climate evolution is well documented within Greenland and Antarctica ice cores (Andersen et al., 2006; EPICA community members, 2004; Grootes et al., 1993; North Greenland Ice Core Project Members et al., 2004; Rasmussen et al., 2006; Svensson et al., 2008; WAIS Divide Project Members et al., 2015; and others) The best chronology for the northern hemisphere is from the annual layer counted NGRIP ice core in Greenland (Rasmussen et al., 2014). These ice core data include also dust (Ruth et al., 2003, 2007). This record is a backbone of dust records, but outside of the chosen regions of the aridity index. Thus, NGRIP-dust was only used in comparison to central European dust.

Several dust proxies were used for this synthesis due to a large variety in dust over the several regions. Calcium carbonate ($CaCO_3$) in the ocean is deposited in higher rates with warmer sea surface temperatures if cores are situated above the lysocline. Therefore, lower $CaCO_3$ contents of ocean sediments in regions of high dust deposition (e.g. deMenocal et al., 2000; Leuschner and Sirocko, 2003) indicate increased mainly aridity, but is also effected by changing wind directions and ocean temperature change. This proxy is thus used only for the construction of the aridity index in Portuguese margin, off west Africa and Arabian Sea.

The grainsize record from the loess plateau in China shows phases of aridity. The larger the sediment grains, the lower the precipitation and temperature and the higher the wind speeds (Sun et al., 2010; Xiao et al., 1995, 2015). Dust or eolian content

of the sediment is given in percentages of the whole sample composition. This is a very robust proxy and used for Australia – Oceania and NW-Africa regions.

In sediments from the Cariaco Basin, the Al/Ti ratio gives the proportion between terrigenous river sediments with higher Al/Ti ratios and Saharan dust with respective lower Al/Ti ratios. Ratio of 14 represent pure Saharan dust (Yarincik et al., 2000). Kaolinite / chlorite (K/C) ratio are a dust proxy for the Mediterranean Sea region (Ehrmann et al., 2017). Higher K/C ratios (more kaolinite than chlorite) indicates increased eolian dust transport. During humid periods, kaolinite was stored within lakes or basins - due to increased erosion - and deflated during arid periods.

2.1 Data treatment and aridity index calculation

We plot all chosen data for a region with a software, written in C++ for the PalMod subproject at Mainz University.(‘*ELSA*interactive ++’ Diensberg, 2020). This software is developed to work with sediment cores on age or depth scale. The time series of speleothem growth phases, tree pollen and dust proxies were resampled to 50 year resolution (by linear interpolation). Afterwards, the resampled datasets were transferred into index values. Therefore, for each timeseries, the data has been recalculated into percentages if the original data was not. Maximum value of each dataset was set to 100%, minimum value was set to 0%, values in between have been normalized.

Speleothem growth phases give information on humid phases, however “no growth” can either indicate changes in the dripwater system or arid conditions. Grass pollen act as a counterpart to tree pollen which indicate humidity. Grass pollen values and dust values are considered to be the more robust aridity proxies, compared to speleothem growth phases. Therefore dust proxies and tree pollen index values were separated into three parts (0, 1, 2) while speleothem growth was only separated into two parts (0, 1). Speleothem growth gets index values of 1, index values of 0 account for no growth. For tree pollen percentages below 33 %, index values were assigned to 0. Tree pollen contents between 33 % and 66 % were assigned to be 1 and larger than 66 % to be index value 2 (see Tab. 1). Dust is considered inverse to tree pollen, higher dust values get assigned lower index values, as lower precipitation and therefore lower soil humidity is the prerequisite for dust deflation. So dust proxy values larger than 66 % are assigned to aridity index value 0, dust proxy values between 33 % and 66 % are assigned to aridity index value 1 and dust proxy values below 33 % are assigned to aridity index value of 2. The index values are then finally summed up.. The aridity index ranges from 0 (highly arid conditions) to 5 (highly humid conditions). Speleothem growth phases, higher tree pollen values and lower dust values combined therefore indicate increased humidity.

The aridity index for all key regions uses always the three proxy types (speleothem growth, tree pollen, dust proxy), except for St. Barbara basin region, where a dust record is not available. For Arabian Sea region, we used TOC as aridity proxy instead of tree pollen, as there were no available pollen data in databases but an excellent organic carbon record. High TOC in the Arabian Sea sediments is caused by high SW-monsoon intensity, intense upwelling and surface water nutrient content, high flux rated of organic matter causing low deep water oxygen content (Schulz, et al., 1998; Sirocko et al., 1993; Sirocko and Ittekkot, 1992).

Speleothems		Tree pollen		Eolian dust	
0	no speleothem growth	0	tree pollen values < 33%	0	dust values > 66%
1	speleothem growth	1	tree pollen values > 33% & < 66%	1	dust values < 66% & > 33%
		2	tree pollen values > 66%	2	dust values < 33%

Table 1. Components of the aridity index: Speleothems can either account as value 0 (no speleothem growth) or 1 (speleothem growth); Tree pollen values below 33 % do not add to the aridity index, between 33 % and 66 % they account for 1 and above 66 % for 2; Dust values were internally normalized and act inverse to tree pollen. Dust values above 66 % do not increase the index, between 66 % and 33 % they count as value 1 and below 33 % as value 2. The aridity index ranges from 0 (highly arid conditions) to 5 (highly humid conditions).

2.2 Error estimates

In general, the main uncertainties of the proxies are the measurements of the original data. In absence of uncertainties for most of the original records, we applied a simple Monte Carlo simulation based on error estimates to get an approximation of the total error. For this we used the error values as displayed in Tab. 2. Speleothem age errors were given in the original data sources. All age-errors of speleothem growth data we used for this synthesis, were below 4 % uncertainty. Errors for pollen and eolian dust were not presented with the original publications; therefore, we had to estimate the uncertainties. These estimates are based on the experience of the ELSA pollen records (Sirocko et al., 2016). To calculate a total error, we randomly disturbed the original data with a probability given by the error estimates and calculated a disturbed aridity index from the disturbed data as described in Tab. 1 and chapter 2.1. The variance over 100 000 runs gives the approximate error of our aridity index. This error simulation is based on Koehler et al. (2009).

The generated error estimations are displayed in Fig. 2 and Figs. S1-S9 by grey colour shades behind the mean data (with 200 year running average) of the aridity index. Hence, aridity index values below 1.5 account for arid conditions, values between 1.5 and 3.5 show intermediate aridity and values larger then 3.5 show more humid conditions (see Fig. 4).

Regions	Speleothem age uncertainty [%]	Tree pollen uncertainty [%]	Eolian dust uncertainty [%]
Central Europe	2.66	3	5
Arabian Sea	1.5	1	3
China	2	2	2
NW-Africa	1	10	2
Southern Europe	1	4	2
Portuguese Margin	1	3	2
Cariaco Basin	4	3	2
Mediterranean Sea	2.5	2	3
St. Barbara Basin	1	3	no dust source
Australia - Oceania	4	3	3

Table 2. Error estimations as input to simulation for all 10 key regions for speleothems, tree pollen and eolian dust.

2.3 Model description

We employ the General Circulation Model COSMOS (community of earth system models) which was developed at the Max-Planck Institute for Meteorology in Hamburg (Jungclaus et al., 2006). COSMOS comprises the standardized IPCC4 model configuration which incorporates the ocean-sea ice model MPIOM (Marsland et al., 2003), the ECHAM5 atmosphere model at T31 spherical resolution (~3.75 × 3.75°) with 19 vertical levels (Roeckner et al., 2003) and the land surface model JSBACH including vegetation dynamics (Brovkin et al., 2009). The ocean model is resolved at 40 unevenly spaced vertical layers and takes advantage of a curve-linear grid at an average resolution of 3 × 1.8° on the horizontal dimension, which increases towards the grid poles at Greenland and Antarctica (~30 km). High-resolution in the realm of the grid poles advances the representation of detailed physical processes at locations of deep-water formation, as Weddell, Labrador and Greenland and Norwegian Seas. The ocean model includes a dynamic-thermodynamic sea-ice model (Hibler, 1979). Net precipitated water over land, which is not stored as snow, intercepted water or soil water, is either interpreted as surface runoff or groundwater and is redirected towards the ocean via a high-resolution river routing scheme (Hagemann and Dümenil, 1997).

Our COSMOS version (COSMOS-landveg r2413, Year 2009) has no flux correction and has been successfully applied to test a variety of paleoclimate hypotheses, ranging from the Cretaceous (Niezgodzki et al., 2017), Miocene climate (Knorr and Lohmann, 2014; Stärz et al., 2017), the Pliocene (Stepanek and Lohmann, 2012), glacial (Gong et al., 2013, 2015; Zhang et al., 2013, 2014) and interglacial climates (Lohmann et al., 2013; Pfeiffer and Lohmann, 2016; Wei and Lohmann, 2012) as well as future climates (Gierz et al., 2015; Lohmann et al., 2008).

Here, we present results obtained from model setups encompassing the Pre-industrial (PI), LGM and late MIS3 (32 000 yr b2k) climate conditions. Details of each experiment set-up have been documented in Wei and Lohmann, 2012 (for PI run), Zhang et al., 2013 (for LGM run) and Gong et al., 2013 (for 32 000 yr b2k run), with modified sea level, ice sheets, greenhouse gas concentrations and Astronomical parameters for their conditions in the past, respectively. For the late MIS3 run, the model mimics a GS due to freshwater hosing and GI with overshoot in temperature (Gong et al., 2013).

3 Results

3.1 Central European climate for the last 60 000 years

The Atlantic sea surface temperature pattern (caused by the Atlantic meridional overturning circulation - AMOC) strongly influence the whole European continent today (e.g. Cassou et al., 2005). Nowadays, the annual mean temperature in Germany is about 9.6 °C and precipitation of about 800 mm/year (Deutscher Wetterdienst, 2018).

An established geoarchive to reconstruct the climate of central are the volcanic maar lakes of the Eifel, which cover the Holocene with varved (annually laminated sediments) and reach back far into the Pleistocene covering the entire last 60 000 years continuously (Sirocko et al., 2016). These maar lakes of the Eifel in western Germany are today up to 70 m deep, with a large water volume and anoxic bottom water, favouring the, preservation of annual layers (Negendank, 1989;

Negendank and Zolitschka, 1993; Zolitschka et al., 2000). We use the long records of the ELSA Project at Mainz University (Sirocko, 2016; Sirocko et al., 2005, 2013) as a starting point for our study. Holocene cores are varved or at least laminated, which leads to a good understanding of sedimentation processes (Sirocko et al., 2016). The LGM and stadial core sections were dominated by sedimentation from annual dust storms (Schaber and Sirocko, 2005), see Fig. 2. The dust index (Dietrich and Seelos, 2010; Dietrich and Sirocko, 2011; Seelos et al., 2009) calculated a dust index which reveals the GIs in detail. The closest known and well dated speleothems to the Eifel region are from the Bunker Cave in Sauerland (Fohlmeister et al., 2012; Weber et al., 2018) which can be compared to the Spannagel Cave system from western Zillertal, Austria (Holzkämper et al., 2004, 2005).

The timespan from 60 000 to 48 000 yr b2k (early MIS3, GIs 17-13) is characterized by a high precipitation visible in the fast speleothem growth of Bunker and Spannagel caves. Nearly 100 % of tree pollen combined with lowest grass and herb pollen values also indicate a wet climate during that time as well as relatively high temperatures close to present day ones (Sirocko et al., 2016). An intermediate dust content in the ELSA-Dust-Stack suggest an intermediate to low aridity, which is supported by a similar pattern of low dust concentration in the NGRIP ice core. This corresponds to underlying common process affecting both regions during this time (most likely the North Atlantic AMOC changes. The pollen composition change in the Eifel began around 49 000 yr b2k towards more grass and herbs pollen. A drastic change in $\delta^{18}O$ occurred at the beginning of GI12 occurred at 46 860 yr b2k (Rasmussen et al., 2014). With the beginning of Heinrich event 5 (HE5), the dust amount spikes in the ELSA-Dust-Stack as well as in the NGRIP core indicating a strong pulse of aridification around 48 000 yr b2k, ending the humid phase of early MIS3.

The period from 48 000 until 38 500 yr b2k comprises GIs 12-9. The speleothem growth in Spannagel ended at 45 700 yr b2k. Bunker Cave speleothem shows a hiatus between 50 000 and 46 000 yr b2k and a short growth recovery with growth ending around 45 000 yr b2k. The tree pollen decreased to about 50 to 60 %, still more tree pollen than grass pollen, but a considerably lower amount than in early MIS3. While the dust amount in the ELSA-Dust-Stack rises to higher intermediate values, the pattern within the NGRIP is characterized by the stadial pulses. ELSA-Dust-Stack, NGRIP dust and NGRIP $\delta^{18}O$ show the same pattern and react apparently to the same mechanism.

From 38 500 to 22 000 yr b2k (GIs 8-2) a change towards lower precipitation and higher aridity occurred. No speleothem growth is documented from Bunker or Spannagel cave. The pollen concentration shows higher grass and herbs content and lower tree pollen percentages, but still some birch and pine trees were present during this time (Sirocko et al., 2016). The ELSA-Dust-Stack comprises of multiple changes within this timespan and shows the general dust content as relatively high with larger variability. The NGRIP in contrast shows the highest dust concentrations in the time between 23 000 and 26 000 yr b2k, a phase where the dust content in the ELSA-Dust-Stack is high, but not at maximum values. The NGRIP $\delta^{18}Oice$ whereas shows a phase of cold temperatures (-45° to -50° C) during this time (Kindler et al., 2014).

The timespan of 22 000 to 14 300 yr b2k also does show no speleothem growth as well as a complete absence of all pollen. The precipitation was at the lowest values of the aridity index for that region, while the ELSA-Dust-Stack shows the highest dust amounts from 23 000 up to 15 000 yr b2k. The biggest difference between ELSA-Dust-Stack and NGRIP-Dust can be

seen in the period of 26 000 to 23 000 yr b2k, where the dust content in the NGRIP core has two distinct maxima, while the dust content in the Central European record increases only slightly. The revival of vegetation followed shortly after 14 300 yr b2k (Litt and Stebich, 1999). Younger Dryas (YD) is apparent in the pollen data by a grass pollen increase and the Holocene is marked by a sharp increase in tree pollen. Throughout the Holocene, tree pollen values range around 90 %. The dust content of the ELSA-Dust-Stack varies between intermediate to low levels. Speleothem growth in Spannagel and Bunker Cave started again at 11 197 (± 94) yr b2k and continues through the whole Holocene. Also, the $\delta^{18}O$ of the NGRIP shows constant high values with exception of the YD event. The time from 14 300 yr b2k up to present day can be described as a humid phase with intermediate to high precipitation and moderate temperatures.

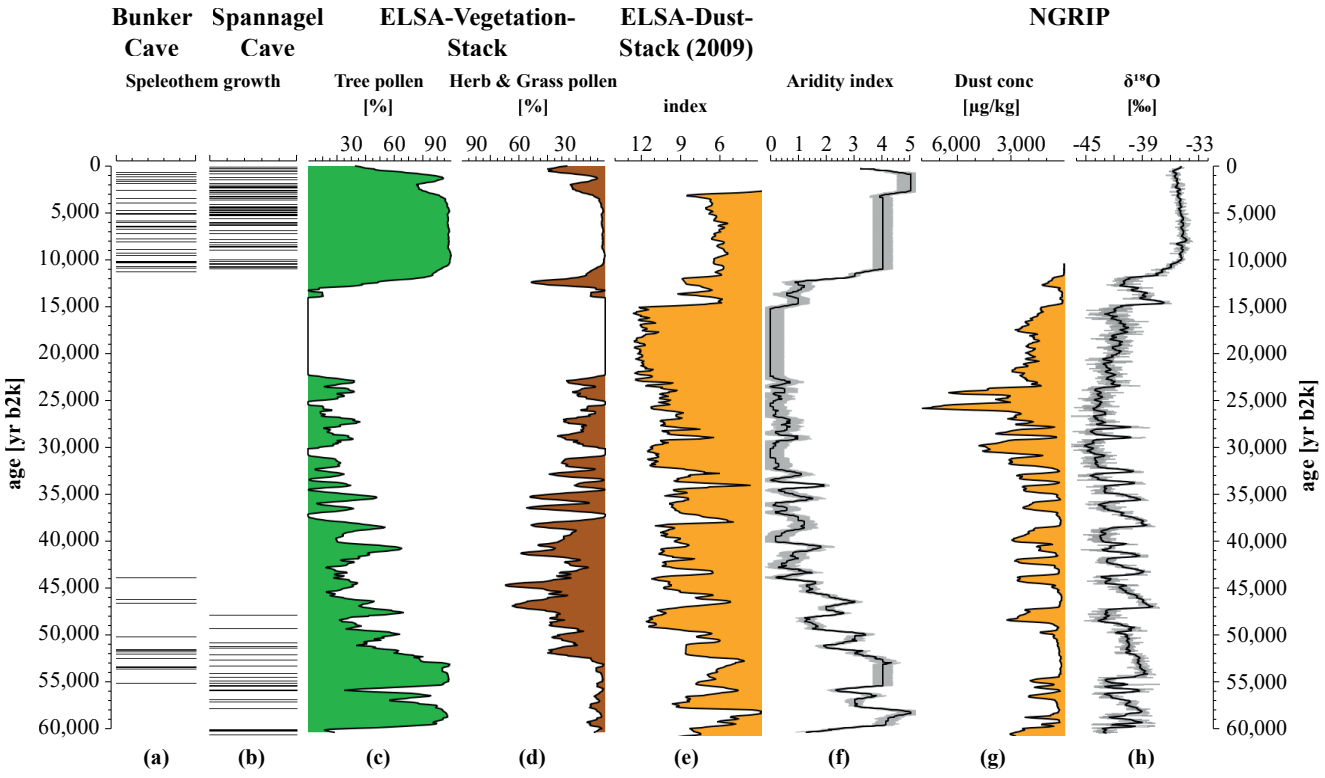

Figure 2: Central European climate over the last 60 000 years: **(a)** Bunker Cave (Fohlmeister et al., 2012, 2013; Weber et al., 2018) and **(b)** Spannagel Cave (Holzkämper et al., 2004, 2005; Spötl and Mangini, 2002) show speleothem growth phases, which require mobile water from frequent precipitation; **(c, d)** ELSA-Vegetation-Stack pollen data (Sirocko et al., 2016) are divided into tree- and herb & grass pollen. While trees require more precipitation, grasses are dominant for more arid conditions; **(e)** ELSA-Dust-Stack (Seelos et al., 2009) indicates more arid conditions with higher values, lower values account for more humid conditions. GIs are distinguishable by lower index values and are highly comparable to **(h)**; **(f)** Aridity index for Central Europe as result from **(a-e)**, for detailed information see method section; **(g)** Dust concentration from NGRIP ice core (Ruth et al., 2007); **(h)** $\delta^{18}O$ data from NGRIP ice core (North Greenland Ice Core Project Members et al., 2004) in comparison.

The Central Europe region is our starting point for the comparison with the nine other key regions, the detailed data description of the other areas is given in the supplement S1-S9.

3.2 Aridity reconstruction of the last 60 000 years

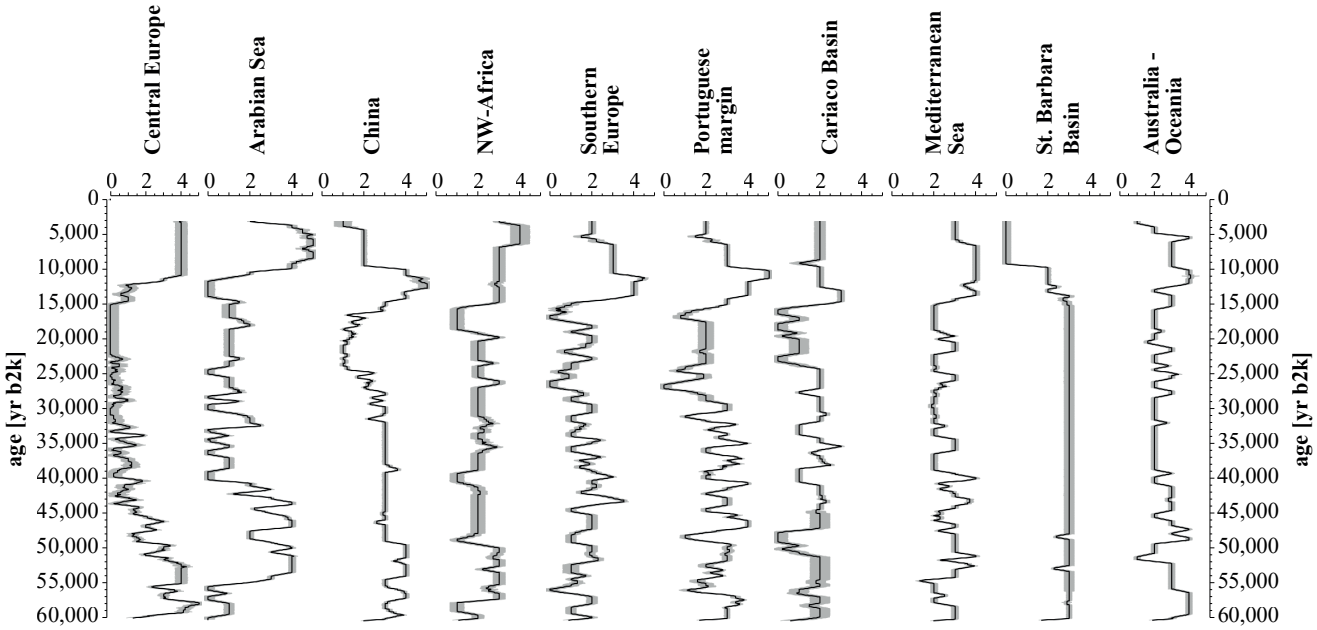

Figure 3: Aridity indices for the 10 key regions over the last 60 000 years. Smaller values indicate more arid, higher values indicate more humid conditions. An early MIS3 wet phase and a Holocene wet phase on various timings for the regions are recognisable.

Figure 3 displays all aridity indices from the regional syntheses. Humid early MIS 3 is apparent for all regions beside Cariaco Basin and St. Barbara Basin, however with offset of several millennia in timings. We cannot ensure if these offset are caused by the stratigraphy or represent leads and lags in the climate system itself. Arid LGM conditions are identifiable for Central Europe, Arabian Sea, China, NW-Africa, Southern Europe, Portuguese margin, Cariaco Basin and Mediterranean Sea region. The last deglaciation is visible in all records by drastic changes around 14 700 yr b2k. A humid phase during Holocene is also apparent for all regions, apart from St. Barbara Basin, where the proxies show an opposing signal to the other archives due to regional effects (see S8 'St. Barbara Basin').

Figure 4 is based on the aridity indices shown in Fig. 3 and additional information of the regional syntheses (see Fig. 2 and S1-S9). For example, publically available pollen data from Mingram et al. (2018) start at 10 150 yr b2k. Pollen reconstructions from Stebich et al. (2015) give additional holocene information on the Sihailongwan maar lake (see S3 'China'). Therefore, we used the additional information after the construction of the aridity index to complete the interpretation shown in Figure 4. Blue bars show humid, yellow bars intermediate and red bars arid conditions. Transitions or subdivisions between these states are marked by both bars overlapping each other. Figure 4 shows three large scale structures that link all 10 selected key areas. The Holocene is in general always relatively humid, but regional variations occur between the early and late Holocene. The time of LGM is arid in all regions of the globe, but the begin of the arid phase starts with large offsets between the 10 regions, which can be again related to stratigraphic inconsistencies or present leads and lags in the regional climate change. The early

MIS3 is quite warm and humid in Europe, south-eastern Asia and Australia, indicating teleconnections between the North Atlantic and the subtropical monsoons (Sirocko et al., 1993).

High humidity is clearly visible for early MIS3 phase for most of the regions apart of the Cariaco basin. The signal is strongest in Central Europe from 60 000 to around 48 000 yr b2k, and in the Arabian Sea from 55 000 to 42 000 yr b2k (Fig. 4 and S1). North-west Africa was less humid in the early MIS3, but still shows enhanced precipitation compared to mid and late MIS3. China and Southern Europe were humid. Portuguese margin region underwent larger changes compared to the other regions, as directly influenced by the North Atlantic. The Mediterranean Sea region also was more humid during mid and late MIS3 but not as humid as other regions, St. Barbara Basin shows humidity with same intensity. The Oceania region shows similar patterns for early MIS3 but with a major decrease in precipitation between 55 000 and 50 000 yr b2k. The early MIS3 was generally quite humid in the northern hemisphere. A pronounced aridification occurred with H5 (around 48 000 yr b2k), especially in NW-Africa, Arabian Sea and Europe.

The time between 45 000 and 15 000 years b2k was globally less humid than the early MIS3 around 50 000 years b2k. Variations occur within the regions during late MIS3, but nevertheless on intermediate or more arid conditions. Heinrich events appear to have a strong impact, especially in the Cariaco Basin where climatic conditions drastically impair during Heinrich events. Towards LGM time, all regions show arid or intermediate conditions, but most arid was again central Europe and the Arabian Sea. The LGM is characterized by decreased precipitation, which is clearly visible by the red bars around 20 000 years b2k (Fig. 4). Oceania conversely shows intermediate values throughout the whole LGM indicating at least some precipitation during the whole period.

Following the LGM, a global climate amelioration took place, again with different timings in the onset for each region due to regional or latitudinal effects. The earliest and most drastic climate improvement took place in China, followed shortly by the Mediterranean region, Central Europe, Southern Europe and Portuguese margin. Also, Cariaco Basin, St. Barbara Basin and Oceania underwent climate improvements even before the Holocene begun. This overall climate improvement is most likely associated with the North Atlantic warming at 14 700 yr b2k (Rasmussen et al., 2014). The Early Holocene Climate Optimum took place with beginning of the Holocene with a temperature and precipitation maximum around 8 000 years b2k (Shakun and Carlson, 2010). This is apparent for Central Europe, Arabian Sea, north-west Africa, Mediterranean Sea, China as well as Australia -Oceania.

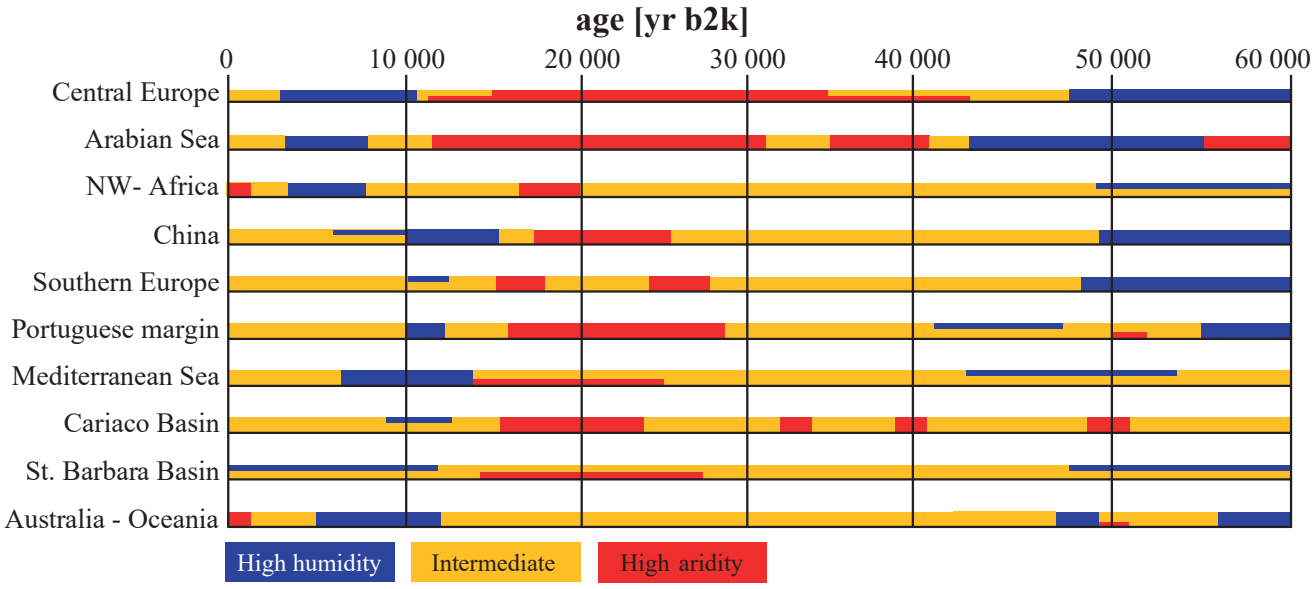

Figure 4: Aridity synthesis for the 10 key regions for the last 60 000 years. Blue bars indicate high humidity, yellow bars intermediate humidity and red bars indicate high aridity. Overlapping half bars indicate transitions between both states. An early MIS3 wet phase and a Holocene wet phase on various timings for the regions are recognisable.

3.3 Global speleothem growth pattern

Figure 5 summarizes all speleothem growth phases mentioned in the regional syntheses. A consistent pattern shows growth of most speleothems during early MIS3 phase, apart from the Bahamas speleothem representative for the Cariaco Basin where speleothem growth started at about 45 000 years b2k. Except for New Zealand, all regions indicate fast growth rates and corresponding humid conditions at least during interstadials. New Zealand shows low growth rates indicating in general more arid conditions. A major change occurs around HE5, shortly after between 48 000 and 45 000 yr b2k respectively. Speleothem growth stopped in Central Europe caves as well as in Arabian Sea region and drastically slowed down in Southern Europe, China and Mediterranean Sea region during late MIS3. The still fast growth for Cariaco Basin could be explained by a regional effect: enhanced moisture supply due to the position of the speleothem on the Bahamas. Climatic conditions impair with progressing time, growth stopped in Cariaco region as well around 23 000 yr b2k. No growth is observed during LGM times for several regions including Central Europe, Arabian Sea, Southern Europe and Cariaco Basin and very slow growth rates are observed for north-west Africa, China and Mediterranean region pointing out to more arid conditions during late MIS3 and LGM times compared to early MIS3 conditions. This also previously observed effect of large-scale atmospheric teleconnections can also be seen by the onset of Bølling / Allerød (14 700 yr b2k) or after YD (11 703 yr b2k), with the restart of speleothem growth for Central Europe, Arabian Sea, Southern Europe, Cariaco Basin and accelerating growth rates like for China, Mediterranean region and Santa Barbara Basin region. The available data show climatic amelioration after LGM globally but especially on the northern hemisphere (NH). Oceania and Southern hemisphere (SH) seem to act as a counterpart

towards the NH. Fast growth rates in Oceania correspond to no or slow growth rates on the northern hemisphere until the Holocene, when both hemispheres show enhanced moisture supply. This shows reverse behaviour between the climate of the hemispheres: If NH receives more precipitation, SHs precipitation decreases and vice versa.

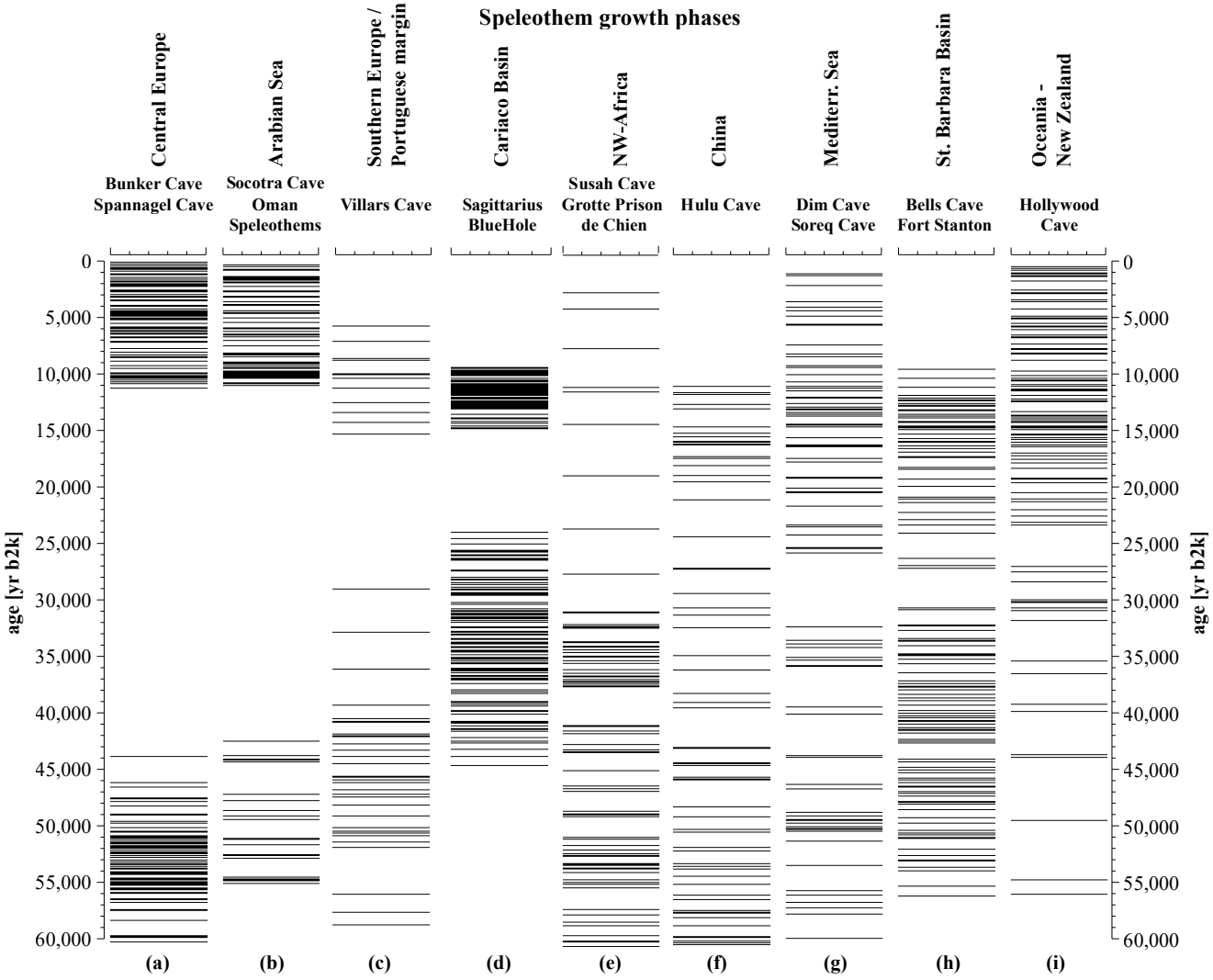

Figure 5: Speleothem growth phases, which require mobile water from frequent precipitation for the 10 key regions. Horizontal bars show age datings. **(a)** Central Europe with Bunker Cave and Spannagel Cave (Fohlmeister et al., 2012, 2013; Holzkämper et al., 2005; Spötl and Mangini, 2002; Weber et al., 2018); **(b)** Socotra Cave and Oman Caves from Arabian Sea region (Burns et al., 2003; Fleitmann et al., 2007); **(c)** Southern Europe and Portuguese margin regions represented by Villars Cave speleothems (Genty et al., 2003, 2006; Wainer et al., 2009); **(d)** Sagittarius Blue Hole Bahamas speleothem for Cariaco Basin region (Hoffmann et al., 2010); **(e)** North-West Africa with Grotte Prison de Chien and Susah Cave (Hoffmann et al., 2016; Wassenburg et al., 2012); **(f)** China with Hulu Cave (Liu et al., 2010; Wang et al., 2001); **(g)** Mediterranean Sea region with Dim Cave and Soreq Cave (Bar-Matthews et al., 2000; Ünal-İmer et al., 2015); **(h)** Bells Cave and Fort Stanton representing St. Barbara Basin (Asmerom et al., 2010; Wagner et al., 2010); **(i)** Hollywood Cave from New Zealand for Oceania region (Hellstrom et al., 1998; Whittaker et al., 2011; Williams, 1996; Williams et al., 2005).

3.4 Global eolian dust pattern

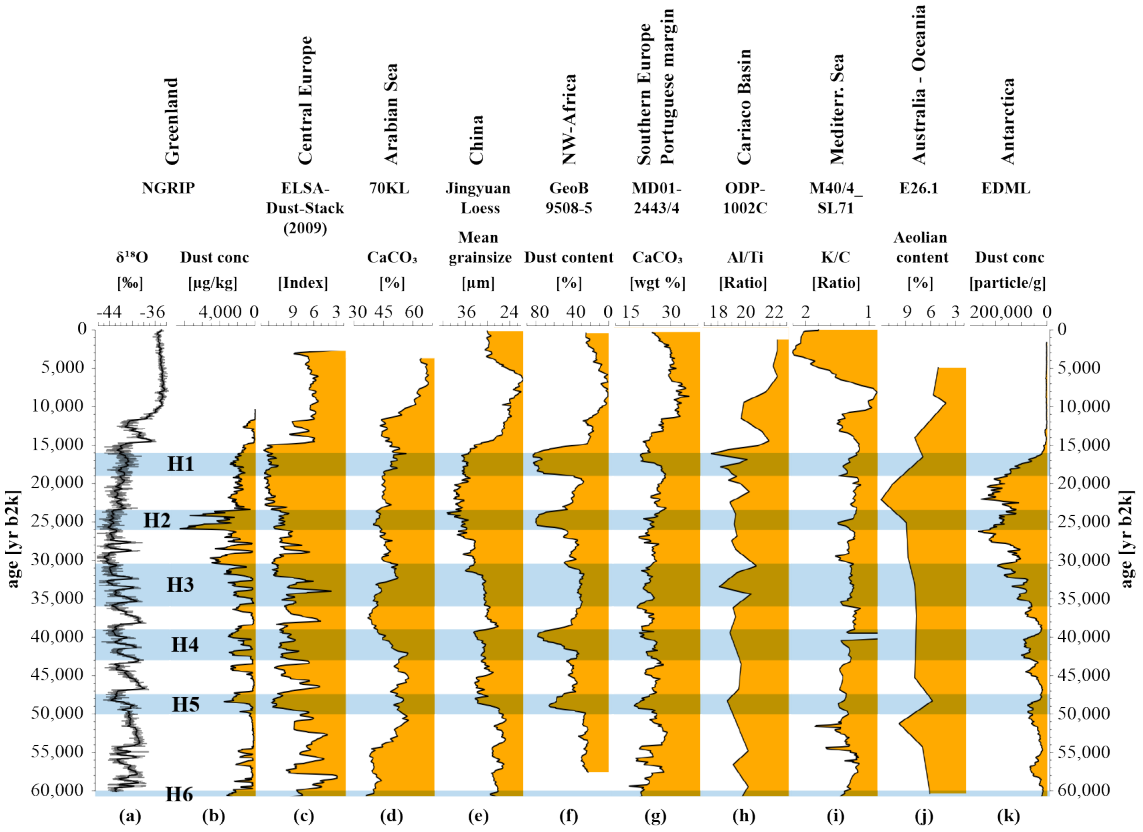

Figure 6: Global eolian dust archives over the last 60 000 years. More dust (left side of each column) indicates increased aridity, less dust indicates increased humidity. **(a)** NGRIP $\delta^{18}O$ (North Greenland Ice Core Project Members et al., 2004) in comparison and **(b)** Dust concentration (Ruth et al., 2007); **(c)** ELSA-Dust-Stack (2009) for Central European dust (Seelos et al., 2009); **(d)** $CaCO_3$ accounting for dust from Arabian Sea marine core 70KL (Leuschner and Sirocko, 2003); **(e)** Mean Grainsize from Jingyuan Chinese Loess plateau (Sun et al., 2010); **(f)** Dust content within marine core GeoB9508-5 off North-West Africa (Collins et al., 2013); **(g)** $CaCO_3$ for Southern Europe and Portuguese margin from marine core MD01-2443/4 (Hodell et al., 2013) **(h)** Cariaco Basin Al/Ti ratio dust record from marine core ODP-165-1002C (Yarincik et al., 2000); **(i)** K/C ratio from marine core M40/4_SL71 for Mediterranean Sea (Ehrmann et al., 2017); **(j)** Aeolian content from marine core E26.1 from Tasmanian Sea for Oceania (Hesse, 1994); **(k)** Antarctica ice core EDML Dust concentration (Wegner et al., 2015) in comparison. Light blue bars highlight Heinrich events after (Naafs et al., 2013).

Similar patterns are visible in the dust archives used for this synthesis. For early MIS3, low dust values are discernible for Central Europe, China, north-west Africa and intermediate dust values for all other regions beside the Arabian Sea. In general, MIS3 climate shows flickering visible within the dust records.

Apart from every region's own pattern, some background structures are apparent. Heinrich events are most pronounced for NW-Africa, Cariaco Basin, Southern Europe and Portuguese margin regions, as these regions directly belong to the North Atlantic. Mediterranean Sea, Central Europe and China also show Heinrich events within the dust records. Cariaco Basin, China, Arabian Sea, NW-Africa and Central Europe show a distinct dust maximum during LGM. Beside during Holocene, the lowest dust values are apparent in the early MIS3 for Central Europe, Arabian Sea, China, NW-Africa and Mediterranean Sea

– but on various timings. NGRIP dust concentration and ELSA-Dust-Stack (Seelos et al., 2009) are in good accordance for early and mid MIS3. Tipping points show stepped appearance in both archives at several times (~49 000, ~36 500, ~23 000, ~14 700 yr b2k) which are also visible and described as Landscape Evolution Zones (LEZ) in Sirocko et al. (2016). The good consistency of both regions indicates a close connection to the North-Atlantic climate variations. Arabian Sea sediments also are closely coupled to North Atlantic variability as known since Schultz et al. (1998) and visible within Fig. 6.

Sun et al. (2010) also shows a correlation of Chinese loess to North Atlantic climate variations. High dust contents during mid MIS3 and LGM are visible in most archives, often related to dustier Heinrich events or stadials in general. Increasing dust values around 30 000 yr b2k towards the LGM show nearly global distribution, but regional differences are observable: ELSA-Dust-Stack and NGRIP differ in the timing of maximum dust values. This could be explained by a similar process like blocking of westerly winds by ice shield growth which is described in Schenk (Schenk et al., 2018) and Schiemann (Schiemann et al., 2017).

From 30 000 to 17 000 yr b2k, the conditions were mainly arid, discernible by the dust maxima in Greenland, Central Europe, China, Portuguese margin, Australia - Oceania and Antarctica for LGM. With the YD and the onset towards the Holocene, global climate ameliorates and dust values decrease globally until the end of the Altithermal. Afterwards, dust increases in Arabian Sea, China, NW-Africa, Portuguese margin and Mediterranean Sea indicating increased aridification of the large desert areas in Africa, Arabian Peninsula and China. Large changes occurred simultaneously on the globe during the last 60 000 years of climate history indicating atmospheric teleconnections (Bjerknes, 1969; Markle et al., 2017; Sirocko, 2003; Sirocko et al., 1993, 1996; Zhou et al., 1999).

4 Discussion

4.1 Comparison of aridity index and previous aridity reconstruction

Aridity reconstructions of Herzschuh (Herzschuh, 2006) for the last 50 000 years for Central Asia are in excellent agreement to the aridity reconstructions of this synthesis of the China region (S3). Herzschuh solely used pollen data for the reconstruction, while our aridity index is based on three distinct proxies to refine the picture. The aridity index in addition consists of longer records and reaches until the beginning of MIS3 (60 000 yr b2k). It shows a humid early MIS3 and a decrease in humidity around 50 000 yr b2k to intermediate conditions. Moderate dry conditions are reconstructed for 50 000 to 45 000 yr b2k from Herzschuh, similar to the aridity index, followed by an increase in humidity until 40 000 yr b2k. Minor differences between 45 000 and 30 000 yr b2k are apparent, but the general trend shows broad consensus between both reconstructions for this time. Mid to late MIS3 are relatively humid in both reconstructions. Aridity increases drastically towards the LGM in both reconstructions with a strong LGM aridity maximum from 21 000 to 18 000 yr b2k. Stepwise climate amelioration after the LGM is clearly expressed in both reconstructions, a first increase in humidity occurs until 13 000 yr b2k with following optimal climate conditions during early Holocene (11 000 - 7 000 yr b2k). The aridity index lacks in Holocene data (see S3) but the accordance of Herzschuh compared to published Holocene pollen data of Stebich (Stebich et al., 2015) is

evident and shows an early Holocene climate optimum until 4 000 yr b2k in both reconstructions. A wet early Holocene can be observed in Central Chinese speleothem growth rates from 'Sanbao Cave', which are highest from 9 500 to 6 500 yr b2k (Dong et al., 2010).

4.2 Comparison of proxy synthesis with model results

The above records describe the structure of past aridity globally, but do not present causal mechanism, which Global Climate Models (GCM) can be used to simulate past, present and future climate changes. In order to our reconstructed precipitation we employ the coupled climate model COSMOS. Fig. 7 displays precipitation changes and anomalies from Late MIS3 time slice with respect to pre-industrial (PI) and LGM conditions. Panel A and C show stadial conditions and panels B and D show interstadial conditions. Panels A and B show the 32 000 yr b2k time slice with respect to pre-industrial times while panels C and D are with respect to LGM conditions.

Model runs for late MIS3 interstadial times show enhanced precipitation for Europe, North Atlantic, Arabian Sea and large parts of the equatorial Pacific, while remaining parts of equator in Asia, Central Atlantic and northern parts of South America show decreased precipitation. Stadial MIS3 state in general shows the same spatial trends but with general higher aridity. Model and aridity reconstructions match in nearly equal conditions for PI and MIS3. Barron and Pollard (2002) simulated a 42 000 yr b2k time slice for European precipitation. The results are comparable to our aridity index, but Central Europe, Southern Europe and Portuguese margin were more humid in our reconstruction than in the simulation of Barron and Pollard. In contrast, these results show that the 42 000 yr b2k time slice was more humid than 32 000 yr b2k time slice for Europe. Our reconstruction estimates precipitation even higher during early and mid than during late MIS3 and to be as high as during early Holocene optimum. This could be said for all regions beside the Cariaco Basin, regarding the different timings of the wet periods. In current models, late MIS3 and especially comparisons between the early and late MIS3 were not investigated so far.

Table 3 summarizes results from the model simulations from Fig. 7, converted into symbols. This model setup is divided in GI and GS state and is compared with the results for the aridity reconstructions from Fig. 4 for each of the ten key regions. Relatively larger aridity with respect to PI or LGM for each region is shown with a minus (-), approximately the same conditions with a circle (o) and more humid conditions with a small plus (+). The agreement of each simulation and the aridity reconstructions of this work is shown in addition. Bad congruence is displayed in red colour, medium with yellow and light and intense green for good and even better accordance respectively. The overall consistence of model and reconstruction is good. Most of the precipitation changes of the aridity index are observable in the simulation as well.

The aridity reconstructions show that Central Europe was humid during early MIS3, followed by an intermediate to highly arid period until the end of LGM.

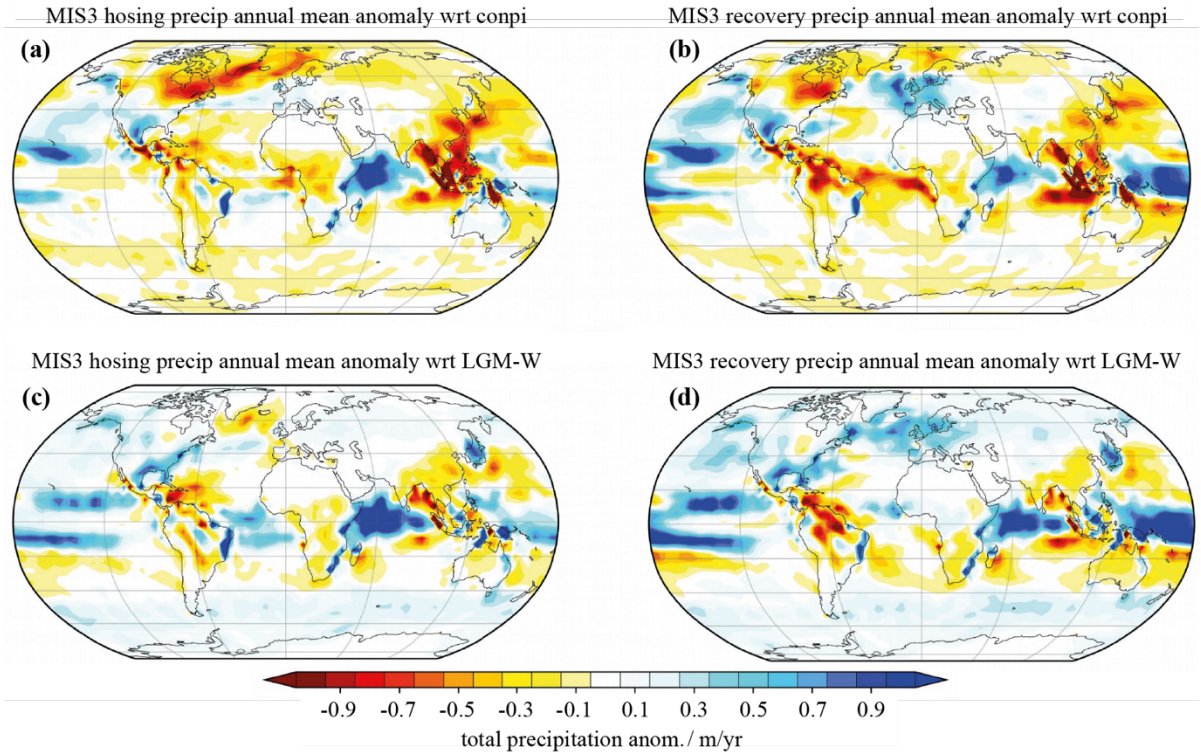

Figure 7: Simulated total precipitation anomalies for the late MIS3 climate relative to pre-industrial times (a, b) or LGM (c, d). Panel **(a, c)** show stadial conditions (hosing) and panels **(b, d)** show interstadial conditions (recovery). Simulation is compiled of various model simulations with COSMOS for pre-industrial (Wei and Lohmann, 2012), LGM (Zhang et al., 2013) and Late MIS3 (32 000 yr b2k) simulations (Gong et al., 2013).

	MIS 3 wrt. PI		MIS 3 wrt. LGM	
	32 000 [a]		32 000 [a]	
	GS	GI	GS	GI
Central Europe	o	+	o	+
Southern Europe	+	+	o	+
Portuguese margin	o	+	o	o
Mediterranean Sea	o	o	o	o
NW Africa	o	o	o	o
China	-	-	-	o
Arabian Sea	+	+	+	o
Cariaco basin	-	-	-	-
St. Barbara basin	o	o	o	o
Australia - Oceania	o	o	o	o

Table 3. Comparison of model simulation with reconstructed aridity index. Relatively larger aridity with respect to PI or LGM for each region is shown with a minus (-), approximately the same conditions with an open circle (o) and more humid conditions with a small plus (+). Bad agreement of simulation and aridity index is shown with red colour, medium by yellow colour, light and intense green account for good or even better accordance respectively.

5 Conclusions

The aridity synthesis for the ten key regions of the world's climate allows six main conclusions to be drawn:

(1) All regions analysed here gone through a wet phase during early MIS3, as well as during the early Holocene. The timing of this humid MIS3 phase varied considerably from region to region.

(2) Atmospheric teleconnections occurred from North Atlantic (Greenland) over Central Europe, Arabian Sea until China. The changes in these regions took place within similar timings and with similar strength. The other regions also went through these changes but with differences in timing. We attribute this to indeed regional effects rather than simply dating uncertainties.

(3) Eolian dust, tree pollen and speleothem growth phases show congruent climatic pattern for the individual regions and can be compared easily regarding precipitation analyses.

(4) The aridity index and the precipitation simulations are generally consistent.

(5) The quality of the aridity index is limited mostly by the original stratigraphy and sample resolution. It is accordingly only a useful tool to observe large scale precipitation changes.

(6) The aridity suggests a general antiphase behaviour between LGM and early MIS3 for northern hemisphere and Australia - Oceania.

Author contributions

FF generated the aridity index, processed the data and prepared the manuscript. GL and XG developed and performed the climate simulation. BD developed the *ELSA*interactive++ program for data visualisation and analysis. Fs stimulated the discussion on the global teleconnections within the climate system.

Acknowledgments

We would like to thank all four anonymous referees which have greatly improved the manuscript. This work was supported by German Federal Ministry of Education and Research (BMBF) as Research for Sustainability initiative (FONA); www.fona.de through PalMod project (FKZ: 01LP1510B). The authors thank Manfred Mudelsee for input on the error estimations, Hannes Knapp, Philip Süßer and Jennifer Klose for data mining, Michael Weber, Johannes Albert, Sarah Britzius for discussion contributions to the manuscript.

References

Andersen, K. K., Svensson, A., Johnsen, S. J., Rasmussen, S. O., Bigler, M., Röthlisberger, R., Ruth, U., Siggaard-Andersen, M.-L., Peder Steffensen, J. and Dahl-Jensen, D.: The Greenland Ice Core Chronology 2005, 15–42ka. Part 1: constructing the

time scale, Quaternary Science Reviews, 25(23–24), 3246–3257, doi:10.1016/j.quascirev.2006.08.002, 2006.

Antoine, P., Rousseau, D.-D., Zöller, L., Lang, A., Munaut, A.-V., Hatté, C. and Fontugne, M.: High-resolution record of the last Interglacial–glacial cycle in the Nussloch loess–palaeosol sequences, Upper Rhine Area, Germany, Quaternary International, 76–77, 211–229, doi:10.1016/S1040-6182(00)00104-X, 2001.

Asmerom, Y., Polyak, V. J. and Burns, S. J.: Variable winter moisture in the southwestern United States linked to rapid glacial climate shifts, Nature Geoscience, 3(2), 114–117, doi:10.1038/ngeo754, 2010.

Bar-Matthews, M., Ayalon, A. and Kaufman, A.: Timing and hydrological conditions of Sapropel events in the Eastern Mediterranean, as evident from speleothems, Soreq cave, Israel, Chemical Geology, 169(1–2), 145–156, 2000.

Barron, E. and Pollard, D.: High-Resolution Climate Simulations of Oxygen Isotope Stage 3 in Europe 1, Quaternary Research, 58(3), 296–309, doi:10.1006/qres.2002.2374, 2002.

Bjerknes, J.: Atmospheric teleconnections from the equatorial pacific, Mon. Wea. Rev., 97(3), 163–172, doi:10.1175/1520-0493(1969)097<0163:ATFTEP>2.3.CO;2, 1969.

Bronk Ramsey, C., Staff, R. A., Bryant, C. L., Brock, F., Kitagawa, H., van der Plicht, J., Schlolaut, G., Marshall, M. H., Brauer, A., Lamb, H. F., Payne, R. L., Tarasov, P. E., Haraguchi, T., Gotanda, K., Yonenobu, H., Yokoyama, Y., Tada, R. and Nakagawa, T.: A Complete Terrestrial Radiocarbon Record for 11.2 to 52.8 kyr B.P., Science, 338(6105), 370–374, doi:10.1126/science.1226660, 2012.

Brovkin, V., Raddatz, T., Reick, C. H., Claussen, M. and Gayler, V.: Global biogeophysical interactions between forest and climate, Geophysical Research Letters, 36(7), doi:10.1029/2009GL037543, 2009.

Burns, S. J., Fleitmann, D., Matter, A., Kramers, J. and Al-Subbary A. A: Indian Ocean Climate and a Absolute Chronology over Dansgaard/Oescher Events 9 to 13, Science, 301, 1365–1367, 2003.

Cassou, C., Terray, L. and Phillips, A. S.: Tropical Atlantic Influence on European Heat Waves, J. Climate, 18(15), 2805–2811, doi:10.1175/JCLI3506.1, 2005.

Clark, P. U., Dyke, A. S., Shakun, J. D., Carlson, A. E., Clark, J., Wohlfarth, B., Mitrovica, J. X., Hostetler, S. W. and McCabe, A. M.: The Last Glacial Maximum, Science, 325(5941), 710–714, doi:10.1126/science.1172873, 2009.

Collins, J. A., Govin, A., Mulitza, S., Heslop, D., Zabel, M., Hartmann, J., Röhl, U. and Wefer, G.: Abrupt shifts of the Sahara-Sahel boundary during Heinrich stadials, Climate of the Past, 9(3), 1181–1191, doi:10.5194/cp-9-1181-2013, 2013.

Correa-Metrio, A., Bush, M. B., Hodell, D. A., Brenner, M., Escobar, J. and Guilderson, T.: The influence of abrupt climate change on the ice-age vegetation of the Central American lowlands: Abrupt climate change in ice-age Central America, Journal of Biogeography, 39(3), 497–509, doi:10.1111/j.1365-2699.2011.02618.x, 2012.

deMenocal, P., Ortiz, J., Guilderson, T., Adkins, J., Sarnthein, M., Baker, L. and Yarusinsky, M.: Abrupt onset and termination of the African Humid Period: rapid climate responses to gradual insolation forcing, Quaternary science reviews, 19(1), 347–361, 2000.

Deutscher Wetterdienst: Wetter und Klima - Deutscher Wetterdienst - Klimadaten weltweit, [online] Available from: https://www.dwd.de/DE/leistungen/klimadatenwelt/klimadatenwelt_node.html (Accessed 17 July 2018), 2018.

Dietrich, S. and Seelos, K.: The reconstruction of easterly wind directions for the Eifel region (Central Europe) during the period 40.3 -12.9 ka BP, Climate of the Past, 6(2), 145–154, doi:10.5194/cp-6-145-2010, 2010.

Dietrich, S. and Sirocko, F.: The potential of dust detection by means of μXRF scanning in Eifel maar lake sediments, Quaternary Science Journal, 60(1), 90–104, doi:10.3285/eg.60.1.06, 2011.

Dong, J., Wang, Y., Cheng, H., Hardt, B., Edwards, R. L., Kong, X., Wu, J., Chen, S., Liu, D., Jiang, X. and Zhao, K.: A high-resolution stalagmite record of the Holocene East Asian monsoon from Mt Shennongjia, central China, The Holocene, 20(2), 257–264, doi:10.1177/0959683609350393, 2010.

Ehrmann, W., Schmiedl, G., Beuscher, S. and Krüger, S.: Intensity of African Humid Periods Estimated from Saharan Dust Fluxes, edited by S.-P. Xie, PLOS ONE, 12(1), e0170989, doi:10.1371/journal.pone.0170989, 2017.

EPICA community members: Eight glacial cycles from an Antarctic ice core, Nature, 429(6992), 623–628, doi:10.1038/nature02599, 2004.

Fleitmann, D., Burns, S. J., Mangini, A., Mudelsee, M., Kramers, J., Villa, I., Neff, U., Al-Subbary, A. A., Buettner, A., Hippler, D. and Matter, A.: Holocene ITCZ and Indian monsoon dynamics recorded in stalagmites from Oman and Yemen (Socotra), Quaternary Science Reviews, 26(1–2), 170–188, doi:10.1016/j.quascirev.2006.04.012, 2007.

Fohlmeister, J., Schröder-Ritzrau, A., Scholz, D., Spötl, C., Riechelmann, D. F. C., Mudelsee, M., Wackerbarth, A., Gerdes, A., Riechelmann, S., Immenhauser, A., Richter, D. K. and Mangini, A.: Bunker Cave stalagmites: an archive for central European Holocene climate variability, Climate of the Past, 8(5), 1751–1764, doi:10.5194/cp-8-1751-2012, 2012.

Fohlmeister, J., Vollweiler, N., Spötl, C. and Mangini, A.: COMNISPA II: Update of a mid-European isotope climate record, 11 ka to present, The Holocene, 23(5), 749–754, doi:10.1177/0959683612465446, 2013.

Genty, D., Blamart, D., Ouahdi, R., Gilmour, M., Baker, A., Jouzel, J. and Van-Exter, S.: Precise dating of Dansgaard–Oeschger climate oscillations in western Europe from stalagmite data, Nature, 421(6925), 833–837, doi:10.1038/nature01391, 2003.

Genty, D., Blamart, D., Ghaleb, B., Plagnes, V., Causse, Ch., Bakalowicz, M., Zouari, K., Chkir, N., Hellstrom, J. and Wainer, K.: Timing and dynamics of the last deglaciation from European and North African δ13C stalagmite profiles—comparison with Chinese and South Hemisphere stalagmites, Quaternary Science Reviews, 25(17–18), 2118–2142, doi:10.1016/j.quascirev.2006.01.030, 2006.

Gierz, P., Lohmann, G. and Wei, W.: Response of Atlantic overturning to future warming in a coupled atmosphere-ocean-ice sheet model, Geophysical Research Letters, 42(16), 6811–6818, doi:10.1002/2015GL065276, 2015.

Gong, X., Knorr, G., Lohmann, G. and Zhang, X.: Dependence of abrupt Atlantic meridional ocean circulation changes on climate background states, Geophysical Research Letters, 40(14), 3698–3704, doi:10.1002/grl.50701, 2013.

Gong, X., Zhang, X., Lohmann, G., Wei, W., Zhang, X. and Pfeiffer, M.: Higher Laurentide and Greenland ice sheets strengthen the North Atlantic ocean circulation, Clim Dyn, 45(1), 139–150, doi:10.1007/s00382-015-2502-8, 2015.

Grimm, E. C., Watts, W. A., Jacobson Jr., G. L., Hansen, B. C. S., Almquist, H. R. and Dieffenbacher-Krall, A. C.: Evidence for warm wet Heinrich events in Florida, Quaternary Science Reviews, 25(17–18), 2197–2211,

doi:10.1016/j.quascirev.2006.04.008, 2006.

Grootes, P. M., Stuiver, M., White, J. W. C., Johnsen, S. and Jouzel, J.: Comparison of oxygen isotope records from the GISP2 and GRIP Greenland ice cores., Nature, 366, 552–554, 1993.

Hagemann, S. and Dümenil, L.: A parametrization of the lateral waterflow for the global scale, Climate Dynamics, 14(1), 17–31, doi:10.1007/s003820050205, 1997.

Hellstrom, J., McCulloch, M. and Stone, J.: A Detailed 31,000-Year Record of Climate and Vegetation Change, from the Isotope Geochemistry of Two New Zealand Speleothems, Quaternary Research, 50(2), 167–178, doi:10.1006/qres.1998.1991, 1998.

Herzschuh, U.: Palaeo-moisture evolution in monsoonal Central Asia during the last 50,000 years, Quaternary Science Reviews, 25(1), 163–178, doi:10.1016/j.quascirev.2005.02.006, 2006.

Hesse, P. P.: The record of continental dust from Australia in Tasman Sea Sediments, Quaternary Science Reviews, 13(3), 257–272, doi:10.1016/0277-3791(94)90029-9, 1994.

Hibler, W. D.: A Dynamic Thermodynamic Sea Ice Model, J. Phys. Oceanogr., 9(4), 815–846, doi:10.1175/1520-0485(1979)009<0815:ADTSIM>2.0.CO;2, 1979.

Hodell, D., Crowhurst, S., Skinner, L., Tzedakis, P. C., Margari, V., Channell, J. E. T., Kamenov, G., Maclachlan, S. and Rothwell, G.: Response of Iberian Margin sediments to orbital and suborbital forcing over the past 420 ka, Paleoceanography, 28(1), 185–199, doi:10.1002/palo.20017, 2013.

Hoffmann, D. L., Beck, J. W., Richards, D. A., Smart, P. L., Singarayer, J. S., Ketchmark, T. and Hawkesworth, C. J.: Towards radiocarbon calibration beyond 28ka using speleothems from the Bahamas, Earth and Planetary Science Letters, 289(1–2), 1–10, doi:10.1016/j.epsl.2009.10.004, 2010.

Hoffmann, D. L., Rogerson, M., Spötl, C., Luetscher, M., Vance, D., Osborne, A. H., Fello, N. M. and Moseley, G. E.: Timing and causes of North African wet phases during the last glacial period and implications for modern human migration, Scientific Reports, 6, 36367, doi:10.1038/srep36367, 2016.

Holzkämper, S., Mangini, A., Spötl, C. and Mudelsee, M.: Timing and progression of the Last Interglacial derived from a high alpine stalagmite: TIMING OF THE LAST INTERGLACIAL, Geophysical Research Letters, 31(7), n/a-n/a, doi:10.1029/2003GL019112, 2004.

Holzkämper, S., Spotl, C. and Mangini, A.: High-precision constraints on timing of Alpine warm periods during the middle to late Pleistocene using speleothem growth periods, Earth and Planetary Science Letters, 236(3–4), 751–764, doi:10.1016/j.epsl.2005.06.002, 2005.

Imbrie, J., Hays, J. D., Martinson, D. G., McIntyre, A., Mix, A. C., Morley, J. J., Pisias, N. G., Prell, W. L. and Shackleton, N. J.: The orbital theory of pleistocene climate: support from a revised chronology of the marine ð18O record, in Milankovitch and Climate, Part 1, edited by A. L. Berger et al, pp. 269–305., 1984.

Jiménez-Moreno, G., Anderson, S. R. and Fawcett, P.: Orbital- and millennial-scale vegetation and climate changes of the past 225ka from Bear Lake, Utah–Idaho (USA), Quaternary Science Reviews, 26(13–14), 1713–1724,

doi:10.1016/j.quascirev.2007.05.001, 2007.

Jungclaus, J. H., Keenlyside, N., Botzet, M., Haak, H., Luo, J.-J., Latif, M., Marotzke, J., Mikolajewicz, U. and Roeckner, E.: Ocean Circulation and Tropical Variability in the Coupled Model ECHAM5/MPI-OM, J. Climate, 19(16), 3952–3972, doi:10.1175/JCLI3827.1, 2006.

Kindler, P., Guillevic, M., Baumgartner, M., Schwander, J., Landais, A., Leuenberger, M., Spahni, R., Capron, E. and Chappellaz, J.: Temperature reconstruction from 10 to 120 kyr b2k from the NGRIP ice core, Climate of the Past, 10(2), 887–902, doi:10.5194/cp-10-887-2014, 2014.

Kliem, P., Enters, D., Hahn, A., Ohlendorf, C., Lisé-Pronovost, A., St-Onge, G., Wastegård, S. and Zolitschka, B.: Lithology, radiocarbon chronology and sedimentological interpretation of the lacustrine record from Laguna Potrok Aike, southern Patagonia, Quaternary Science Reviews, 71, 54–69, doi:10.1016/j.quascirev.2012.07.019, 2013.

Knorr, G. and Lohmann, G.: Climate warming during Antarctic ice sheet expansion at the Middle Miocene transition, Nature Geoscience, 7(5), 376–381, doi:10.1038/ngeo2119, 2014.

Koehler, E., Brown, E. and Haneuse, S. J.-P. A.: On the Assessment of Monte Carlo Error in Simulation-Based Statistical Analyses, Am Stat, 63(2), 155–162, doi:10.1198/tast.2009.0030, 2009.

Leuschner, D. C. and Sirocko, F.: Orbital insolation forcing of the Indian Monsoon - a motor for global climate changes?, Palaeogeography Palaeoclimatology Palaeoecology, 197(1–2), 83–95, 2003.

Litt, T. and Stebich, M.: Bio- and chronostratigraphy of the lateglacial in the Eifel region, Germany, Quaternary International, 61(1), 5–16, doi:10.1016/S1040-6182(99)00013-0, 1999.

Liu, D., Wang, Y., Cheng, H., Lawrence Edwards, R., Kong, X., Wang, X., Hardt, B., Wu, J., Chen, S., Jiang, X., He, Y., Dong, J. and Zhao, K.: Sub-millennial variability of Asian monsoon intensity during the early MIS 3 and its analogue to the ice age terminations, Quaternary Science Reviews, 29(9), 1107–1115, doi:10.1016/j.quascirev.2010.01.008, 2010.

Lohmann, G., Haak, H. and Jungclaus, J. H.: Estimating trends of Atlantic meridional overturning circulation from long-term hydrographic data and model simulations, Ocean Dynamics, 58(2), 127–138, doi:10.1007/s10236-008-0136-7, 2008.

Lohmann, G., Pfeiffer, M., Laepple, T., Leduc, G. and Kim, J.-H.: A model-data comparison of the Holocene global sea surface temperature evolution, Climate of the Past, 1807–1839, doi:Lohmann, G. ORCID: https://orcid.org/0000-0003-2089-733X <https://orcid.org/0000-0003-2089-733X>, Pfeiffer, M. , Laepple, T. ORCID: https://orcid.org/0000-0001-8108-7520 <https://orcid.org/0000-0001-8108-7520>, Leduc, G. and Kim, J. H. (2013) A model-data comparison of the Holocene global sea surface temperature evolution , Climate of the Past, (9), pp. 1807-1839 . doi:https://doi.org/10.5194/cp-9-1807-2013 <https://doi.org/10.5194/cp-9-1807-2013> , hdl:10013/epic.41917, 2013.

Markle, B. R., Steig, E. J., Buizert, C., Schoenemann, S. W., Bitz, C. M., Fudge, T. J., Pedro, J. B., Ding, Q., Jones, T. R., White, J. W. C. and Sowers, T.: Global atmospheric teleconnections during Dansgaard–Oeschger events, Nature Geoscience, 10(1), 36–40, doi:10.1038/ngeo2848, 2017.

Marsland, S. J., Haak, H., Jungclaus, J. H., Latif, M. and Röske, F.: The Max-Planck-Institute global ocean/sea ice model with orthogonal curvilinear coordinates, Ocean Modelling, 5(2), 91–127, doi:10.1016/S1463-5003(02)00015-X, 2003.

Martinson, D. G., Pisias, N. G., Hays, J. D., Imbrie, J., Moore jr., T. C. and Shackelton, N. J.: Age Dating and the Orbital Theory of the Ice Ages: Development of a High-Resolution 0 to 300,000-Year Chronostratigraphy, Quaternary Researche, 27, 1–29, 1987.

McManus, J. F., Bond, G. C., Broecker, W. S., Johnsen, S., Labeyrie, L. and Higgins, S.: High-resolution climate records from the North Atlantic during the last interglacial, Nature, 371(6495), 326, doi:10.1038/371326a0, 1994.

Mingram, J., Stebich, M., Schettler, G., Hu, Y., Rioual, P., Nowaczyk, N., Dulski, P., You, H., Opitz, S., Liu, Q. and Liu, J.: Millennial-scale East Asian monsoon variability of the last glacial deduced from annually laminated sediments from Lake Sihailongwan, N.E. China, Quaternary Science Reviews, 201, 57–76, doi:10.1016/j.quascirev.2018.09.023, 2018.

Mix, A. C., Bard, E. and Schneider, R.: Environmental processes of the ice age: land, oceans, glaciers (EPILOG), Quaternary Science Reviews, 20(4), 627–657, doi:10.1016/S0277-3791(00)00145-1, 2001.

Moine, O., Antoine, P., Hatté, C., Landais, A., Mathieu, J., Prud'homme, C. and Rousseau, D.-D.: The impact of Last Glacial climate variability in west-European loess revealed by radiocarbon dating of fossil earthworm granules, Proceedings of the National Academy of Sciences, 114(24), 6209–6214, doi:10.1073/pnas.1614751114, 2017.

Naafs, B. D. A., Hefter, J., Grützner, J. and Stein, R.: Warming of surface waters in the mid-latitude North Atlantic during Heinrich events: HIGH SSTs DURING HEINRICH EVENTS, Paleoceanography, 28(1), 153–163, doi:10.1029/2012PA002354, 2013.

Negendank, J. F. W.: Pleistozäne und holozäne Maarsedimente der Eifel, Zeitschrift der Deutschen Geologischen Gesellschaft, 13–24, 1989.

Negendank, J. F. W. and Zolitschka, B.: Maars and maar lakes of the Westeifel Volcanic Field, in Paleolimnology of European Maar Lakes, edited by J. F. W. Negendank and B. Zolitschka, pp. 61–80, Springer Berlin Heidelberg, Berlin, Heidelberg., 1993.

Niezgodzki, I., Knorr, G., Lohmann, G., Tyszka, J. and Markwick, P. J.: Late Cretaceous climate simulations with different CO2 levels and subarctic gateway configurations: A model-data comparison, Paleoceanography, 32(9), 980–998, doi:10.1002/2016PA003055, 2017.

North Greenland Ice Core Project Members, Andersen, K. K., Azuma, N., Barnola, J.-M., Bigler, M., Biscaye, P., Caillon, N., Chappellaz, J., Clausen, H. B., Dahl-Jensen, D., Fischer, H., Flückiger, J., Fritzsche, D., Fujii, Y., Goto-Azuma, K., Grønvold, K., Gundestrup, N. S., Hansson, M., Huber, C., Hvidberg, C. S., Johnsen, S. J., Jonsell, U., Jouzel, J., Kipfstuhl, S., Landais, A., Leuenberger, M., Lorrain, R., Masson-Delmotte, V., Miller, H., Motoyama, H., Narita, H., Popp, T., Rasmussen, S. O., Raynaud, D., Rothlisberger, R., Ruth, U., Samyn, D., Schwander, J., Shoji, H., Siggard-Andersen, M.-L., Steffensen, J. P., Stocker, T., Sveinbjörnsdóttir, A. E., Svensson, A., Takata, M., Tison, J.-L., Thorsteinsson, T., Watanabe, O., Wilhelms, F. and White, J. W. C.: High-resolution record of Northern Hemisphere climate extending into the last interglacial period, Nature, 431(7005), 147–151, doi:10.1038/nature02805, 2004.

Pfeiffer, M. and Lohmann, G.: Greenland Ice Sheet influence on Last Interglacial climate: global sensitivity studies performed with an atmosphere–ocean general circulation model, Climate of the Past, 1313–1338, 2016.

Pross, J., Koutsodendris, A., Christanis, K., Fischer, T., Fletcher, W. J., Hardiman, M., Kalaitzidis, S., Knipping, M., Kotthoff, U., Milner, A. M., Müller, U. C., Schmiedl, G., Siavalas, G., Tzedakis, P. C. and Wulf, S.: The 1.35-Ma-long terrestrial climate archive of Tenaghi Philippon, northeastern Greece: Evolution, exploration, and perspectives for future research, , doi:info:doi/10.1127/nos/2015/0063, 2015.

Pye, K.: Aeolian dust and dust deposits., Academic Press, University of Cambridge., 1987.

Rasmussen, S. O., Andersen, K. K., Svensson, A. M., Steffensen, J. P., Vinther, B. M., Clausen, H. B., Siggaard-Andersen, M.-L., Johnsen, S. J., Larsen, L. B., Dahl-Jensen, D., Bigler, M., Röthlisberger, R., Fischer, H., Goto-Azuma, K., Hansson, M. E. and Ruth, U.: A new Greenland ice core chronology for the last glacial termination, Journal of Geophysical Research, 111(D6), doi:10.1029/2005JD006079, 2006.

Rasmussen, S. O., Bigler, M., Blockley, S. P., Blunier, T., Buchardt, S. L., Clausen, H. B., Cvijanovic, I., Dahl-Jensen, D., Johnsen, S. J., Fischer, H., Gkinis, V., Guillevic, M., Hoek, W. Z., Lowe, J. J., Pedro, J. B., Popp, T., Seierstad, I. K., Steffensen, J. P., Svensson, A. M., Vallelonga, P., Vinther, B. M., Walker, M. J. C., Wheatley, J. J. and Winstrup, M.: A stratigraphic framework for abrupt climatic changes during the Last Glacial period based on three synchronized Greenland ice-core records: refining and extending the INTIMATE event stratigraphy, Quaternary Science Reviews, 106, 14–28, doi:10.1016/j.quascirev.2014.09.007, 2014.

Roeckner, E., Bäuml, G., Bonaventura, L., Brokopf, R., Esch, M., Giorgetta, M., Hagemann, S., Kirchner, I., Kornblueh, L., Manzini, E., Rhodin, A., Schlese, U., Schulzweida, U. and Tompkins, A.: The atmospheric general circulation model ECHAM 5. PART I: Model description, , doi:10.17617/2.995269, 2003.

Ruth, U., Wagenbach, D., Steffensen, J. P. and Bigler, M.: Continuous record of microparticle concentration and size distribution in the central Greenland NGRIP ice core during the last glacial period: CONTINUOUS RECORD OF MICROPARTICLE CONCENTRATION, Journal of Geophysical Research: Atmospheres, 108(D3), n/a-n/a, doi:10.1029/2002JD002376, 2003.

Ruth, U., Bigler, M., Röthlisberger, R., Siggaard-Andersen, M.-L., Kipfstuhl, S., Goto-Azuma, K., Hansson, M. E., Johnsen, S. J., Lu, H. and Steffensen, J. P.: Ice core evidence for a very tight link between North Atlantic and east Asian glacial climate, Geophysical Research Letters, 34(3), doi:10.1029/2006GL027876, 2007.

Schaber, K. and Sirocko, F.: Lithologie und Stratigraphie der spätpleistozänen Trockenmaare der Eifel, Mainzer geowissenschaftliche Mitteilungen, 33, 295–340, 2005.

Schenk, F., Väliranta, M., Muschitiello, F., Tarasov, L., Heikkilä, M., Björck, S., Brandefelt, J., Johansson, A. V., Näslund, J.-O. and Wohlfarth, B.: Warm summers during the Younger Dryas cold reversal, Nature Communications, 9(1), doi:10.1038/s41467-018-04071-5, 2018.

Schiemann, R., Demory, M.-E., Shaffrey, L. C., Strachan, J., Vidale, P. L., Mizielinski, M. S., Roberts, M. J., Matsueda, M., Wehner, M. F. and Jung, T.: The resolution sensitivity of Northern Hemisphere blocking in four 25-km atmospheric global circulation models, Journal of Climate, 30, 337–358, 2017.

Schulz, H., von Rad, U., Erlenkeuser, H. and von Rad, U.: Correlation between Arabian Sea and Greenland climate oscillations

of the past 110,000 years, Nature, 393(6680), 54–57, doi:10.1038/31750, 1998.

Seelos, K., Sirocko, F. and Dietrich, S.: A continuous high-resolution dust record for the reconstruction of wind systems in central Europe (Eifel, Western Germany) over the past 133 ka, Geophysical Research Letters, 36(20), doi:10.1029/2009GL039716, 2009.

Shakun, J. D. and Carlson, A. E.: A global perspective on Last Glacial Maximum to Holocene climate change, Quaternary Science Reviews, 29(15), 1801–1816, doi:10.1016/j.quascirev.2010.03.016, 2010.

Sirocko, F.: What Drove Past Teleconnections?, Science, 301(5638), 1336–1337, doi:10.1126/science.1088626, 2003.

Sirocko, F.: The ELSA - Stacks (Eifel-Laminated-Sediment-Archive): An introduction, Global and Planetary Change, 142, 96–99, doi:10.1016/j.gloplacha.2016.03.011, 2016.

Sirocko, F. and Ittekkot, V.: Organic carbon accumulation rates in the Holocene and Glacial Arabian Sea: Implications for the global CO2 budget., Climate Dynamics, 7, 167–172, 1992.

Sirocko, F., Sarnthein, M., Erlenkeuser, H., Lange, H., Arnold, M. and Duplessy, J. C.: Century-scale events in monsoonal climate over the past 24,000 years, Nature, 364(6435), 322, doi:10.1038/364322a0, 1993.

Sirocko, F., Garbe-Schönberg, D., McIntyre, A. and Molfino, B.: Teleconnections Between the Subtropical Monsoons and High-Latitude Climates During the Last Deglaciation, Science, 272(5261), 526–529, doi:10.1126/science.272.5261.526, 1996.

Sirocko, F., Seelos, K., Schaber, K., Rein, B., Dreher, F., Diehl, M., Lehne, R., Jager, K., Krbetschek, M. and Degering, D.: A late Eemian aridity pulse in central Europe during the last glacial inception, Nature, 436(7052), 833–836, doi:10.1038/nature03905, 2005.

Sirocko, F., Dietrich, S., Veres, D., Grootes, P. M., Schaber-Mohr, K., Seelos, K., Nadeau, M.-J., Kromer, B., Rothacker, L., Roehner, M., Krbetschek, M., Appleby, P., Hambach, U., Rolf, C., Sudo, M. and Grim, S.: Multi-proxy dating of Holocene maar lakes and Pleistocene dry maar sediments in the Eifel, Germany, Quat. Sci. Rev., 62, 56–76, doi:10.1016/j.quascirev.2012.09.011, 2013.

Sirocko, F., Knapp, H., Dreher, F., Förster, M. W., Albert, J., Brunck, H., Veres, D., Dietrich, S., Zech, M., Hambach, U., Röhner, M., Rudert, S., Schwibus, K., Adams, C. and Sigl, P.: The ELSA-Vegetation-Stack: Reconstruction of Landscape Evolution Zones (LEZ) from laminated Eifel maar sediments of the last 60,000years, Global and Planetary Change, 142, 108–135, doi:10.1016/j.gloplacha.2016.03.005, 2016.

Spötl, C. and Mangini, A.: Stalagmite from the Austrian Alps reveals Dansgaard–Oeschger events during isotope stage 3: Implications for the absolute chronology of Greenland ice cores, Earth and Planetary Science Letters, 203(1), 507–518, doi:10.1016/S0012-821X(02)00837-3, 2002.

Stärz, M., Jokat, W., Knorr, G. and Lohmann, G.: Threshold in North Atlantic-Arctic Ocean circulation controlled by the subsidence of the Greenland-Scotland Ridge, Nature Communications, 8(1), 1–13, doi:10.1038/ncomms15681, 2017.

Stebich, M., Rehfeld, K., Schlütz, F., Tarasov, P. E., Liu, J. and Mingram, J.: Holocene vegetation and climate dynamics of NE China based on the pollen record from Sihailongwan Maar Lake, Quaternary Science Reviews, 124, 275–289, doi:https://doi.org/10.1016/j.quascirev.2015.07.021, 2015.

Stepanek, C. and Lohmann, G.: Modelling mid-Pliocene climate with COSMOS, Geosci. Model Dev., 5, 1221–1243, doi:Stepanek, C. ORCID: https://orcid.org/0000-0002-3912-6271 <https://orcid.org/0000-0002-3912-6271> and Lohmann, G. ORCID: https://orcid.org/0000-0003-2089-733X <https://orcid.org/0000-0003-2089-733X> (2012) Modelling mid-Pliocene climate with COSMOS , Geosci. Model Dev., 5 , pp. 1221-1243 . doi:https://doi.org/10.5194/gmd-5-1221-2012 <https://doi.org/10.5194/gmd-5-1221-2012> , hdl:10013/epic.39137, 2012.

Sun, Y., Wang, X., Liu, Q. and Clemens, S. C.: Impacts of post-depositional processes on rapid monsoon signals recorded by the last glacial loess deposits of northern China, Earth and Planetary Science Letters, 289(1–2), 171–179, doi:10.1016/j.epsl.2009.10.038, 2010.

Svensson, A., Andersen, K. K., Bigler, M., Clausen, H. B., Dahl-Jensen, D., Davies, S. M., Johnsen, S. J., Muscheler, R., Parrenin, F., Rasmussen, S. O., Röthlisberger, R., Seierstad, I., Steffensen, J. P. and Vinther, B. M.: A 60 000 year Greenland stratigraphic ice core chronology, Clim. Past, 12, 2008.

Thompson, W. G. and Goldstein, S. L.: A radiometric calibration of the SPECMAP timescale, Quaternary Science Reviews, 25(23), 3207–3215, doi:10.1016/j.quascirev.2006.02.007, 2006.

Újvári, G., Stevens, T., Svensson, A., Klötzli, U. S., Manning, C., Németh, T., Kovács, J., Sweeney, M. R., Gocke, M., Wiesenberg, G. L. B., Markovic, S. B. and Zech, M.: Two possible source regions for central Greenland last glacial dust: SOURCE REGIONS OF GREENLAND GLACIAL DUST, Geophysical Research Letters, 42(23), 10,399-10,408, doi:10.1002/2015GL066153, 2015.

Ünal-İmer, E., Shulmeister, J., Zhao, J.-X., Tonguç Uysal, I., Feng, Y.-X., Duc Nguyen, A. and Yüce, G.: An 80 kyr-long continuous speleothem record from Dim Cave, SW Turkey with paleoclimatic implications for the Eastern Mediterranean, Scientific Reports, 5(1), doi:10.1038/srep13560, 2015.

Wagner, J. D. M., Cole, J. E., Beck, J. W., Patchett, P. J., Henderson, G. M. and Barnett, H. R.: Moisture variability in the southwestern United States linked to abrupt glacial climate change, Nature Geoscience, 3(2), 110–113, doi:10.1038/ngeo707, 2010.

Wainer, K., Genty, D., Blamart, D., Hoffmann, D. and Couchoud, I.: A new stage 3 millennial climatic variability record from a SW France speleothem, Palaeogeography, Palaeoclimatology, Palaeoecology, 271(1–2), 130–139, doi:10.1016/j.palaeo.2008.10.009, 2009.

WAIS Divide Project Members, Buizert, C., Adrian, B., Ahn, J., Albert, M., Alley, R. B., Baggenstos, D., Bauska, T. K., Bay, R. C., Bencivengo, B. B., Bentley, C. R., Brook, E. J., Chellman, N. J., Clow, G. D., Cole-Dai, J., Conway, H., Cravens, E., Cuffey, K. M., Dunbar, N. W., Edwards, J. S., Fegyveresi, J. M., Ferris, D. G., Fitzpatrick, J. J., Fudge, T. J., Gibson, C. J., Gkinis, V., Goetz, J. J., Gregory, S., Hargreaves, G. M., Iverson, N., Johnson, J. A., Jones, T. R., Kalk, M. L., Kippenhan, M. J., Koffman, B. G., Kreutz, K., Kuhl, T. W., Lebar, D. A., Lee, J. E., Marcott, S. A., Markle, B. R., Maselli, O. J., McConnell, J. R., McGwire, K. C., Mitchell, L. E., Mortensen, N. B., Neff, P. D., Nishiizumi, K., Nunn, R. M., Orsi, A. J., Pasteris, D. R., Pedro, J. B., Pettit, E. C., Buford Price, P., Priscu, J. C., Rhodes, R. H., Rosen, J. L., Schauer, A. J., Schoenemann, S. W., Sendelbach, P. J., Severinghaus, J. P., Shturmakov, A. J., Sigl, M., Slawny, K. R., Souney, J. M., Sowers, T. A., Spencer, M.

K., Steig, E. J., Taylor, K. C., Twickler, M. S., Vaughn, B. H., Voigt, D. E., Waddington, E. D., Welten, K. C., Wendricks, A. W., White, J. W. C., Winstrup, M., Wong, G. J. and Woodruff, T. E.: Precise interpolar phasing of abrupt climate change during the last ice age, Nature, 520(7549), 661–665, doi:10.1038/nature14401, 2015.

Wang, Y. J., Cheng, H., Edwards, R. L., An, Z. S., Wu, J. Y., Shen, C.-C. and Dorale, J. A.: A High-Resolution Absolute-Dated Late Pleistocene Monsoon Record from Hulu Cave, China, Science, 294(5550), 2345, doi:10.1126/science.1064618, 2001.

Wassenburg, J. A., Immenhauser, A., Richter, D. K., Jochum, K. P., Fietzke, J., Deininger, M., Goos, M., Scholz, D. and Sabaoui, A.: Climate and cave control on Pleistocene/Holocene calcite-to-aragonite transitions in speleothems from Morocco: Elemental and isotopic evidence, Geochimica et Cosmochimica Acta, 92, 23–47, doi:10.1016/j.gca.2012.06.002, 2012.

Weber, M., Scholz, D., Schroeder-Ritzrau, A., Deininger, M., Spoetl, C., Lugli, F., Mertz-Kraus, R., Jochum, K. P., Fohlmeister, J., Stumpf, C. F. and Riechelmann, D. F. C.: Evidence of warm and humid interstadials in central Europe during early MIS 3 revealed by a multi-proxy speleothem record, Quat. Sci. Rev., 200, 276–286, doi:10.1016/j.quascirev.2018.09.045, 2018.

Wegner, A., Fischer, H., Delmonte, B., Petit, J.-R., Erhardt, T., Ruth, U., Svensson, A., Vinther, B. and Miller, H.: The role of seasonality of mineral dust concentration and size on glacial/interglacial dust changes in the EPICA Dronning Maud Land ice core: EPICA DML DUST RECORD, Journal of Geophysical Research: Atmospheres, 120(19), 9916–9931, doi:10.1002/2015JD023608, 2015.

Wei, W. and Lohmann, G.: Simulated Atlantic Multidecadal Oscillation during the Holocene, J. Climate, 25(20), 6989–7002, doi:10.1175/JCLI-D-11-00667.1, 2012.

Wessel, P. and Smith, W. H. F.: Free software helps map and display data, Eos, Transactions American Geophysical Union, 72(41), 441–446, doi:10.1029/90EO00319, 1991.

Whittaker, T. E., Hendy, C. H. and Hellstrom, J. C.: Abrupt millennial-scale changes in intensity of Southern Hemisphere westerly winds during marine isotope stages 2–4, Geology, 39(5), 455–458, doi:10.1130/G31827.1, 2011.

Williams, P. W.: A 230 ka record of glacial and interglacial events from Aurora Cave, Fiordland, New Zealand, New Zealand Journal of Geology and Geophysics, 39(2), 225–241, doi:10.1080/00288306.1996.9514707, 1996.

Williams, P. W., King, D. N. T., Zhao, J.-X. and Collerson, K. D.: Late Pleistocene to Holocene composite speleothem 18O and 13C chronologies from South Island, New Zealand—did a global Younger Dryas really exist?, Earth and Planetary Science Letters, 230(3–4), 301–317, doi:10.1016/j.epsl.2004.10.024, 2005.

Xiao, J., Porter, S. C., An, Z., Kumai, H. and Yoshikawa, S.: Grain Size of Quartz as an Indicator of Winter Monsoon Strength on the Loess Plateau of Central China during the Last 130,000 Yr, Quaternary Research, 43(1), 22–29, doi:10.1006/qres.1995.1003, 1995.

Xiao, M., Zhang, Q. and Singh, V. P.: Influences of ENSO, NAO, IOD and PDO on seasonal precipitation regimes in the Yangtze River basin, China, International Journal of Climatology, 35(12), 3556–3567, doi:10.1002/joc.4228, 2015.

Yarincik, K. M., Murray, R. W. and Peterson, L. C.: Climatically sensitive eolian and hemipelagic deposition in the Cariaco

Basin, Venezuela, over the past 578,000 years: Results from Al/Ti and K/Al, Paleoceanography, 15(2), 210–228, doi:10.1029/1999PA900048, 2000.

Zhang, X., Lohmann, G., Knorr, G. and Xu, X.: Different ocean states and transient characteristics in Last Glacial Maximum simulations and implications for deglaciation, Climate of the Past, 9(5), 2319–2333, doi:10.5194/cp-9-2319-2013, 2013.

Zhang, X., Lohmann, G., Knorr, G. and Purcell, C.: Abrupt glacial climate shifts controlled by ice sheet changes, Nature, 512(7514), 290–294, doi:10.1038/nature13592, 2014.

Zhou, W., Head, M. J., Lu, X., An, Z., Jull, A. J. T. and Donahue, D.: Teleconnection of climatic events between East Asia and polar, high latitude areas during the last deglaciation, Palaeogeography, Palaeoclimatology, Palaeoecology, 152(1), 163–172, doi:10.1016/S0031-0182(99)00041-3, 1999.

Zolitschka, B., Brauer, A., Negendank, J. F. W., Stockhausen, H. and Lang, A.: Annually dated late Weichselian continental paleoclimate record from the Eifel, Germany, Geology, 28(9), 783–786, doi:10.1130/0091-7613(2000)28<783:ADLWCP>2.0.CO;2, 2000.